PNAS RESEARCH ARTICLE | APPLIED BIOLOGICAL SCIENCES

Metabolic engineering of *Bacillus subtilis* for the production of active hemoglobins and myoglobins by improving heme supply

Song Wang[a,b,c,d,e], Jingwen Zhou[a,b,c,d], Jianghua Li[a,b,c,d], Jian Chen[a,b,c,d], Guocheng Du[a,b,c,d], Zhengqiang Li[e], Sang Yup Lee[f,1], and Xinrui Zhao[a,b,c,d,1]

Affiliations are included on p. 10.

Contributed by Sang Yup Lee; received March 4, 2025; accepted June 4, 2025; reviewed by Irina Borodina and Michael C. Jewett

Hemoglobins (Hb) and myoglobins (Mb) are important hemoproteins with broad applications in food and medicine. Microbial cell factory is a promising approach for the green and sustainable production of hemoproteins. However, current microbial hosts face the challenges of safety and insufficient heme supply. Here, we report a global regulation strategy, "push–restrain–pull–block," to enhance heme supply for producing various active Hb and Mb in food-grade *Bacillus subtilis*. Initially, the insufficient supply of the precursor 5-aminolevulinate was overcome by relieving feedback inhibition and mitigating the negative effects of HemX on HemA. Next, HemD was identified as the primary uroporphyrinogen III synthase and self-assembled with HemC to minimize the formation of the uroporphyrinogen I by-product. Additionally, the coproporphyrin-dependent pathway was selected as the superior downstream route for heme synthesis, and crucial rate-limiting steps were subsequently enhanced. Moreover, heme consumption was blocked by eliminating protoheme IX farnesyltransferase. Finally, through the combination and fine-tuned expression of key genes, a 221-fold improvement of heme supply was achieved in the engineered strain. Using this stable prokaryotic chassis, we achieved production of 0.81, 0.82, 1.11, and 1.01 g L^{-1} of soybean Hb, clover Hb (C-Hb), bovine Mb (B-Mb), and porcine Mb, respectively, through fermentation, marking the highest reported titers in prokaryotic systems. These hemoproteins exhibit properties similar to natural standards. Furthermore, the synthesized C-Hb and B-Mb demonstrated superior effects for preparing plant-based meat analogs as colorants and flavoring agents. This work provides a universal platform for producing other high-value hemoproteins, promising future advancements in food processing and biocatalysis.

Bacillus subtilis | heme supply | push–restrain–pull–block | active hemoproteins | microbial cell factory

Significance

The large-scale biosynthesis of active hemoproteins for applications in the manufacture of food and medicine remains a significant challenge. In this study, we comprehensively identified bottlenecks in the heme biosynthetic pathway and addressed them using a "push–restrain–pull–block" strategy. Based on these metabolic modifications, we developed a stable food-grade *Bacillus subtilis* chassis with efficient and moderate heme supply. Consequently, various active hemoglobins (Hb) and myoglobins (Mb) were successfully produced, achieving higher titers and productivities. Additionally, the biosynthesized clover Hb and bovine Mb demonstrated excellent properties for enhancing the color and flavor of plant-based meat analogs. This work lays a foundation for scalable biosynthesis of valuable hemoproteins used in food technology, healthcare, and green chemistry.

Hemoglobin (Hb) and myoglobin (Mb) consist of globin and heme, playing crucial roles in applications such as acellular oxygen carriers, iron supplements, and biocatalysis (1–3). Also, they are considered key colorants and flavoring agents in animal-derived meat products (4, 5). Incorporating Hb and Mb into meat analogs significantly enhances their flavor profiles, making them more akin to real meat (6, 7). Notably, soybean Hb (S-Hb) has received approval from the United States Food and Drug Administration as a color and flavor additive (GRN No. 737) and is used by Impossible Foods Inc. in plant-based ground beef analogs (8). Bovine Mb (B-Mb) and porcine Mb (P-Mb) offer potential for realistic meat-like coloration in plant-based and cell-based artificial meat analogs (5, 9). Previous research indicates that clover Hb (C-Hb) outperforms S-Hb as a color additive due to its retention of red color even when oxidized (10).

Meeting the increasing demand and commercial value of Hb and Mb, traditional chemical extraction faces limitations in efficiency, sustainability, and environmental impact (11). Advances in metabolic engineering have led to the development of microbial cell factories for the production of Hb and Mb (12–14), offering a promising avenue for large-scale, efficient, and environmentally friendly production. Currently, yeast expression systems have achieved the highest reported titers of S-Hb (7.3 g L^{-1} in *Kluyveromyces marxianus*), P-Mb (296.6 mg L^{-1} in *Pichia pastoris*), C-Hb (13.7 mg L^{-1} in *Saccharomyces cerevisiae*), and B-Mb (68.9 mg L^{-1} in *S. cerevisiae*) (14–16). However, these systems are hindered by slower growth rates and longer fermentation durations, increasing the risk of contamination and elevating production costs. Additionally, *S. cerevisiae* exhibits generally low production titers of hemoprotein (14), and *P. pastoris* requires methanol induction for recombinant protein expression, raising safety concerns regarding the final product (16). Although *K. marxianus* demonstrates promising S-Hb titers and enhanced biosafety, the absence of data on

Reviewers: I.B., Danmarks Tekniske Universitet; and M.C.J., Northwestern University.

The authors declare no competing interest.

[1]To whom correspondence may be addressed. Email: leesy@kaist.ac.kr or zhaoxinrui@jiangnan.edu.cn.

This article contains supporting information online at https://www.pnas.org/lookup/suppl/doi:10.1073/pnas.2504795122/-/DCSupplemental.

Published July 2, 2025.

heme-binding ratio and enzymatic activity raises concerns regarding its commercial viability (15). Furthermore, the relatively poor plasmid stability in *K. marxianus* restricts its potential for use in industrial-scale hemoprotein production. Despite *Escherichia coli*'s advantages of short fermentation period and high production of S-Hb and human Hb, the risk of endotoxin contamination remains significant (12, 17). In contrast, *Bacillus subtilis* exhibits rapid growth, shorter fermentation times (~24 h), and advantages in industrial production due to robust fermentation capabilities and higher expression levels of heterogenous proteins (18). Moreover, *B. subtilis* has no endotoxin risk and has been widely used in food and pharmaceutical applications (19).

Heme plays crucial roles as an essential cofactor in the proper folding and functions of hemoproteins (20). In *B. subtilis* (Fig. 1), the heme biosynthetic pathway begins with the synthesis of 5-aminolevulinic acid (ALA) via the C5 pathway involving glutamyl-tRNA reductase GtrR (encoded by *hemA*) and glutamate-1-semialdehyde 2,1-aminomutase GsaM (encoded by *hemL* and *gsaB*). ALA is then converted to hydroxymethylbilane (HMB) by porphobilinogen synthase PbgS (encoded by *hemB*) and HMB synthase HmbS (encoded by *hemC*). Subsequently, uroporphyrinogen III (UPG III) is formed from HMB through cyclization catalyzed by UPG III synthase UroS. In *B. subtilis*, three genes (*hemD*, *nasF*, and *yjjA*) encode potential enzymes with UroS activity. UPG III decarboxylase UroD (encoded by *hemE*) then converts UPG III to coproporphyrinogen III (CPG III). Finally, CPG III is converted to heme through the coproporphyrin-dependent (CPD) pathway by CPG III oxidase CgoX (encoded by *hemY*), coproporphyrin ferrochelatase CpfC (encoded by *hemH*), and coproheme decarboxylase ChdC (encoded by *hemQ*) (21). Additionally, according to the Kyoto Encyclopedia of Genes and Genomes (KEGG) database, a protoporphyrin-dependent (PPD) pathway has been annotated in *B. subtilis*. However, authentic CpdH has not been found in sequenced genomes of Firmicutes (including *B. subtilis*) and Actinobacteria, suggesting that heme synthesis via the PPD pathway may not occur in *B. subtilis* (22). Further evidence from other Gram-positive bacteria indicates that HemN and HemZ may have been misannotated as CpdH (23), further casting doubt on the functionality of PPD pathway in *B. subtilis*.

Sufficient heme supply is essential for producing active Hb and Mb (13). While exogenous addition of ALA or heme has been attempted to enhance Hb and Mb activities, these approaches increase costs and are limited by transport into the cell (24). An alternative, more efficient, and cost-effective strategy involves improving endogenous heme supply through metabolic engineering. Current engineering strategies primarily involve overexpressing all genes or key genes in the heme synthetic pathway based on previous research (14, 25–27). However, these strategies are not universally applicable due to species-specific bottlenecks in the heme biosynthetic pathway. A metabolic model-based customized approach has been reported to predict and modify potential heme synthesis-related genes, but this approach led to significant growth

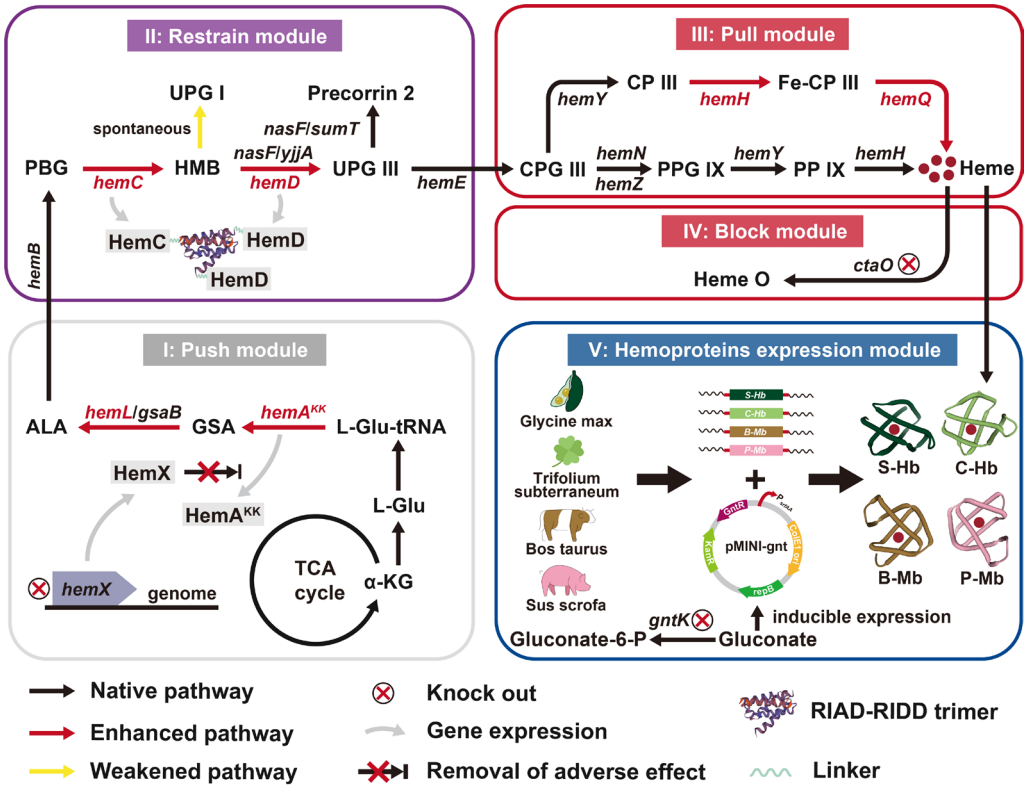

Fig. 1. An overview of metabolic engineering strategies for stepwise enhancing heme supply to produce active hemoglobins and myoglobins. I: pushing more carbon flux into the heme synthetic pathway; II: restraining the competitive consumption of HMB intermediates in the heme synthetic pathway; III: pulling the flow of CPG III toward heme synthesis; IV: blocking the downstream conversion of heme; V: synthesizing active hemoproteins. Abbreviations: α-KG, α-ketoglutarate; L-Glu, L-glutamate; L-Glu-tRNA, L-glutamate-tRNA; *hemA*^{KK} encodes glutamyl-tRNA reductase inserted two lysine residues (KK) between the second and the third residues; *hemX* encodes protein HemX; GSA, glutamate-1-semialdehyde; *hemL* and *gsaB* encode glutamate-1-semialdehyde 2,1-aminomutase; ALA, 5-aminolevulinic acid; *hemB* encodes porphobilinogen synthase; PBG, porphobilinogen; *hemC* encodes HMB synthase; HMB, hydroxymethylbilane; UPG I, uroporphyrinogen I, UPG III, uroporphyrinogen III, *hemD* and *yjjA* encode UPG III synthase; *nasF* encodes UPG III methyltransferase/synthase; *sumT* encodes UPG III methyltransferase; *hemE* encodes UPG III decarboxylase; CPG III, coproporphyrinogen III; *hemY* encodes protoporphyrinogen/CPG III oxidase; CP III, coproporphyrin III; *hemH* encodes protoporphyrin/coproporphyrin ferrochelatase; Fe-CP III, Fe-coproporphyrin III; *hemQ* encodes coproheme decarboxylase; *hemN* and *hemZ* encode oxygen-independent CPG III oxidase; PPG IX, protoporphyrinogen IX; PP IX, protoporphyrin IX; *ctaO* encodes protoheme IX farnesyltransferase; *gntK* encodes gluconate kinase; S-Hb, soybean hemoglobin; C-Hb, clover hemoglobin; B-Mb, bovine myoglobin; P-Mb, porcine myoglobin.

inhibition, likely due to metabolic burden and accumulation of harmful intermediate metabolites (26). Another strategy involves constructing strains without significant accumulation of intermediate metabolites by overexpressing different combinations of genes in the heme synthetic pathway using plasmids (28). However, this approach yielded only 2.46 mg L^{-1} heme and resulted in over 50% inhibition of cell growth. Generally, previous strategies often overlooked metabolic burden and intermediate metabolite accumulation, necessitating careful consideration of these factors to optimize engineered chassis cells for active Hb and Mb production.

Here, we performed systems metabolic engineering for the development of an engineered *B. subtilis* chassis with enhanced heme supply for synthesizing active Hb and Mb. Specifically, we optimized heme biosynthesis by increasing ALA precursor supply, minimizing uroporphyrinogen I (UPG I) by-product formation, selecting the CPD pathway for superior heme synthesis, enhancing the crucial rate-limiting steps, and blocking heme consumption. Employing an appropriate expression strategy for globins, our engineered strain successfully synthesized active Hb and Mb in shake-flask and fed-batch fermentations. Furthermore, the biosynthesized Hb and Mb positively influenced the color and flavor of plant-based meat analogs.

Results

Engineering the C5 Pathway to Increase Carbon Flux into Heme Biosynthesis. After optimizing plasmid copy number and expression type for globin expression, the pMINI-gntR plasmid (high copy number, gluconate-inducible expression) was selected for the expression of globin (*SI Appendix*, Fig. S1*B* and Text S1). The wild-type *B. subtilis* strains harboring the plasmid to express hemoproteins achieved titers of 187.36 ± 4.05 mg L^{-1} for S-Hb, 200.65 ± 10.11 mg L^{-1} for C-Hb, 227.09 ± 7.53 mg L^{-1} for B-Mb, and 276.98 ± 15.78 mg L^{-1} for P-Mb (*SI Appendix*, Fig. S1*C*). Additionally, the heme-binding rates for these hemoproteins were 15.59 ± 2.02%, 13.72 ± 1.34%, 22.37 ± 1.91%, and 15.33 ± 0.42%, respectively (*SI Appendix*, Fig. S1*E*). Clearly, the wild-type strain could not meet the heme demand for synthesized Hb and Mb, prompting investigation into enhancing endogenous heme supply through engineered pathways.

The heme biosynthetic pathway in *B. subtilis* (Fig. 1) is divided into four modules: I) push module, II) restrain module, III) pull module, and IV) block module. To assess the heme synthetic pathway in wild-type *B. subtilis*, various metabolites were monitored at 24 and 48 h in shake-flask cultivation using high-performance liquid chromatography (HPLC). All tested intermediate metabolites and heme were below HPLC detection limits (*SI Appendix*, Table S1), mirroring results from other wild-type hosts (29, 30), indicating low metabolic flux through the heme biosynthetic pathway (Fig. 2*A*). The bottleneck in the push module was insufficient ALA supply, the initial precursor for heme synthesis. Therefore, enhancing the C5 pathway was pursued to increase carbon flux into heme biosynthesis.

Initially, *hemA* and *hemL* from *B. subtilis* 168, *E. coli* BL21, and *Corynebacterium glutamicum* ATCC 14067 were overexpressed via plasmid pHT01. Given that GsaB may function similarly to GsaM,

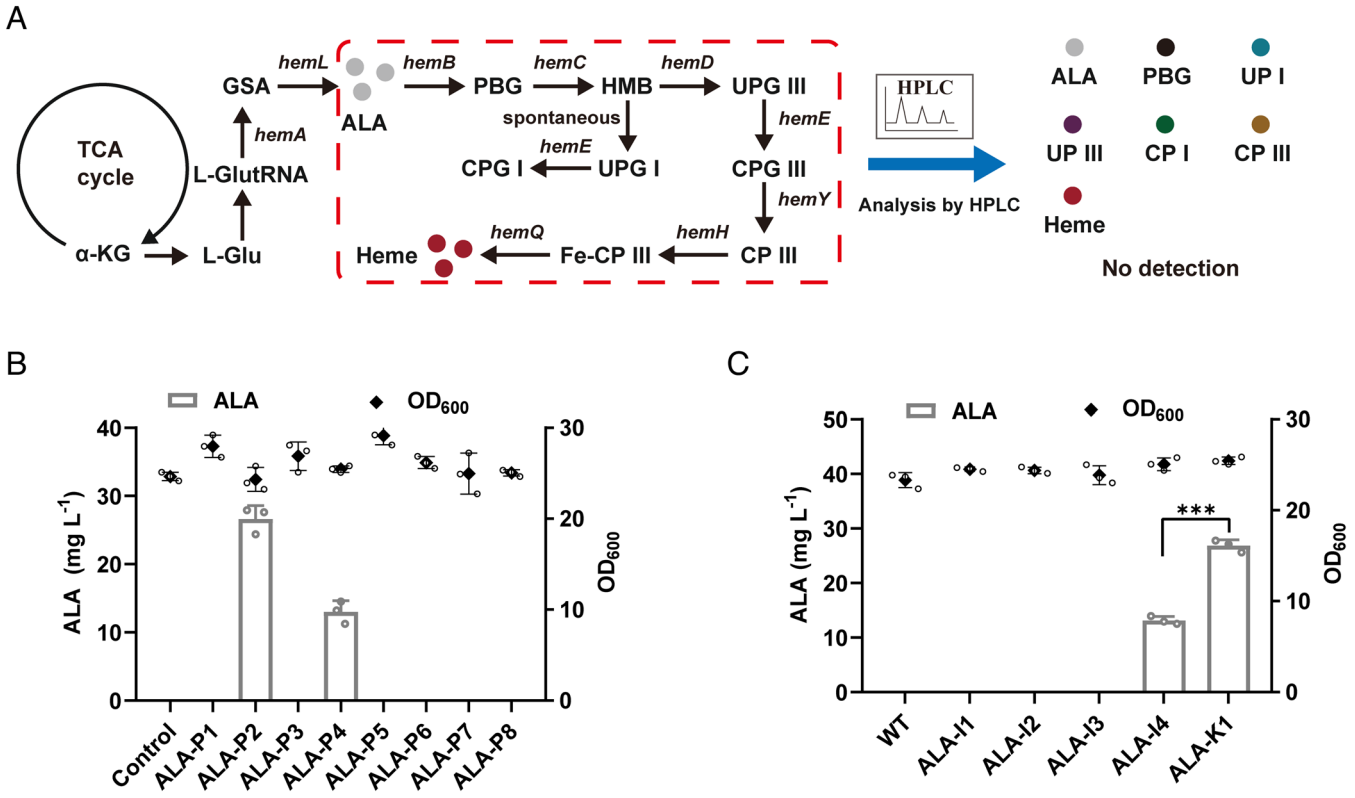

Fig. 2. Identification of key bottlenecks in the heme biosynthetic pathway and increasing the supply of ALA to push more carbon flux into the heme biosynthetic pathway. (*A*) Schematic illustration of metabolic flux analysis (MFA) for intermediates in the heme biosynthetic pathway, analyzed by HPLC. The abbreviations are shown in Fig. 1. (*B*) Screening of C5 pathways derived from different strains through overexpression using the pHT01 plasmid. Control: wild-type strain harboring empty pHT01 plasmid; strains ALA-P1 to P8: wild-type strain harboring pHT01-hemAL-*B. subtilis*, pHT01-hemA^{KK}L-*B. subtilis*, pHT01-hemAgsaB-*B. subtilis*, pHT01-hemA^{KK}gsaB-*B. subtilis*, pHT01-hemAL-*C. glutamicum*, pHT01-hemA^{KK}L-*C. glutamicum*, pHT01-hemAL-*E. coli*, pHT01-hemA^{KK}L-*E. coli*, respectively. (*C*) Optimal promoter screening of the *hem*A^{KK}-*hemL* cassette for chromosomal integration, and effect of the *hemX* gene knockout on ALA accumulation. WT: wild-type *B. subtilis*; strains ALA-I1 to I4: *amyE*::P_{sdhB}-*hem*A^{KK}*L*, *amyE*::P_{43}-*hem*A^{KK}*L*, *amyE*::P_{yvyD}-*hem*A^{KK}*L*, *amyE*::P_{veg}-*hem*A^{KK}*L*, respectively; ALA-K1 strain: knocking out the *hemX* gene from the ALA-I4 strain. The bars and solid symbols present as mean values ± SD from three independent biological replicates (n = 3). Hollow circles represent individual data points. *$P < 0.05$, **$P < 0.01$, ***$P < 0.001$; ns, no significance.

according to KEGG database annotations, *gsaB* was also validated. To prevent proteolysis-mediated feedback inhibition (31), two lysine residues (KK) were inserted between the second and third residues of HemA, generating $HemA^{KK}$. Shake-flask cultivation of the ALA-P2 strain, a wild-type strain harboring pHT01-$hemA^{KK}$L-*B. subtilis,* in BSM medium yielded the highest ALA titer of 26.63 ± 1.96 mg L^{-1} in 24 h (Fig. 2*B*). Thus, overexpression of $hemA^{KK}$ and *hemL* was deemed necessary to enhance the C5 pathway flux. Furthermore, as shown in Fig. 2*B*, ALA production by the ALA-P2 strain significantly exceeded that of the ALA-P4 strain (wild-type strain harboring pHT01-$hemA^{KK}$gsaB-*B. subtilis*), suggesting that HemL primarily functions as GsaM in *B. subtilis*.

Genome-scale redesign of metabolic pathways is crucial for mitigating metabolic burden and enhancing strain genetic stability (32, 33). Subsequently, endogenous $hemA^{KK}$-*hemL* cassettes, controlled by promoters (P_{sdhB}, P_{43}, P_{veg}, and P_{yvyD}) of varying strengths, were integrated into the classical *amyE* locus of the wild-type strain using the CRISPR-Cas9 system, resulting in strains ALA-I1 to ALA-I4. ALA production was assessed across these strains with different $hemA^{KK}$-*hemL* cassettes. The P_{veg} promoter was selected for expressing $hemA^{KK}$-*hemL* cassettes (ALA-I4 strain), yielding the highest ALA accumulation of 13.13 ± 0.72 mg L^{-1} at 24 h (Fig. 2*C*). Additionally, the membrane protein HemX negatively impacts HemA concentration in *B. subtilis* (34). Consequently, knocking out the *hemX* gene in the ALA-I4 strain produced higher ALA titers (26.84 ± 1.12 mg L^{-1}) at 24 h, 2.11-fold higher than the ALA-I4 strain (Fig. 2*C*). Based on these results, the ALA-K1 strain was selected for further engineering.

Weakening the Competitive Pathway to Redirect Metabolic Flux Toward Heme Biosynthesis. According to the "push–pull" theory, increasing downstream pull typically promotes the conversion of upstream metabolites (35). Consequently, although the ALA-K1 strain exhibited a certain level of ALA accumulation (Fig. 2*C*), the *hemB* gene was not considered for overexpression here. To explore the bottleneck of ALA flow to CPG III, the accumulation of uroporphyrins was detected at 24 and 48 h after supplementing the fermentation medium with exogenous ALA (2 g L^{-1}) at 12 h for the wild-type strain (Fig. 3*A*). The results showed that the accumulation of uroporphyrin I (UP I) exceeded that of UP III by over sevenfold (*SI Appendix*, Fig. S2), indicating that metabolic flux in the heme biosynthetic pathway was predominantly diverted toward competitive pathways. HMB rapidly autocyclizes to UPG I unless UroS captures it by reversing the terminal ring to synthesize UPG III (36). Additionally, UPG I is oxidized to UP I after being released from cells (36). Therefore, the key bottleneck in the "restrain module" was the consumption of metabolic flux caused by the autocyclization of HMB.

The authentic activity of UroS may be attributed to HemD, NasF, and YjjA in *B. subtilis*, according to annotations in the KEGG database. Thus, a trienzymatic reaction system (containing PbgS, HmbS, and UroS) was constructed to identify the authentic UroS (*SI Appendix*, Fig. S3*A*). Five enzymes were purified, including HemB, HemC, HemD, NasF, and YjjA with 6× His tag at their C termini (*SI Appendix*, Fig. S3*B*). Subsequently, HemB and HemC were pretreated at 60 °C for 10 min to eliminate any contamination of UroS due to their remarkable thermal stability (37, 38). Three potential UroS enzymes (HemD, YjjA, or NasF) were then incubated with HemB and HemC at a molar ratio of 1:5:5 in a reaction system containing excess ALA for 15 min (Fig. 3*B*). The results revealed that the reaction system containing HemD produced the highest accumulation of UP III, while there was almost no UP III accumulation in the other groups, demonstrating that the HemD possessed the activity of UroS (Fig. 3*B*).

To accelerate the conversion of HMB to UPG III, a pair of short peptide tags (RIAD and RIDD) capable of assembling scaffold-free enzymes were used to narrow the spatial spacing between HemC and HemD (39, 40). RIAD and RIDD were respectively fused to HemC and HemD, spaced by a flexible linker $(G_4S)_2G_4CG$. The short peptide tags fused to the N- or C-terminus of target proteins affected the catalytic reactions provided by the enzyme complex (41). Here, the effect of RIAD and RIDD attached to the N-terminal or C-terminal of HemC and HemD on the reduction of HMB consumption was examined. Plasmids harboring different combinations of cassettes were transformed into wild-type *B. subtilis*, generating strains UP-P2 to UP-P5. Similarly, 2 g L^{-1} ALA was added to the fermentation medium at 12 h, and the accumulations of UP I and UP III were detected at 36 h. According to the evaluation criterion of UP I accumulation and the ratio of UP III and UP I, the RIDD-HemD-HemC-RIAD combination (RIDD at HemD N terminus and RIAD at HemC C-terminus) was regarded as the optimal connection mode (Fig. 3 *C* and *D*). Compared to the UP-P1 strain (overexpressing the *hemC* and *hemD* genes), the UP-P3 strain (overexpressing *RIDD-hemD-hemC-RIAD* cassette) showed a 32.58% reduction in UP I accumulation and a 1.64-fold increase in UP III accumulation (Fig. 3*C*). This finding indicates that constructing a dual-enzyme complex can effectively promote the conversion of HMB to UPG III. To avoid the metabolic burden caused by plasmid-based expression and inappropriate expression levels of *RIDD-hemD-hemC-RIAD* cassette, this cassette was integrated into the *amyE* locus of the ALA-K1 strain under the control of different constitutive promoters (P_{sdhB}, P_{yvyD}, and P_{556}). Compared with the ALA-K1 strain (Fig. 3*E*), the P_{yvyD} promoter was selected for expressing the *RIDD-hemD-hemC-RIAD* cassette (UP-I2 strain), resulting in a 36.88% reduction in UP I accumulation. In addition, there were 1.71-fold and 17.37-fold increase in the accumulations of UP III and coproporphyrin III (CP III) at 48 h, respectively.

The endogenous HemC, without the fused RIAD short peptide tag, cannot assemble with RIDD-HemD. To further reduce the conversion of HMB to UPG I, the endogenous *hemC* gene in the UP-I2 strain was knocked out to create the UP-K1 strain. As expected, the accumulations of UP III and CP III increased by 1.40- and 1.36-fold, respectively (Fig. 3*F*). Moreover, UPG III is converted to precorrin-2 by UPG III methyltransferase (SumT), encoded by the *nasF* and *sumT* genes in most Gram-positive bacteria (42). Thus, the *nasF* and *sumT* genes were knocked out from the genome of the UP-K1 strain to weaken the competing pathways of UPG III. However, the UP-K2 (knockout of the *nasF* gene) and UP-K3 (knockout of the *sumT* gene) strains did not show positive effects on the accumulation of CP III (*SI Appendix*, Fig. S4), possibly due to existing UPG III in the UP-K1 strain inhibiting the activity of SumT (43). Finally, based on the same considerations as those for the *hemB* gene, the *hemE* gene was also not overexpressed. Consequently, the obtained UP-K1 strain was used as a chassis cell for the further design of metabolic pathway and the subsequent optimization to increase heme supply.

Enhancing the Rate-Limiting Steps in the CPD Pathway and Eliminating Heme Consumption. In microorganisms, three heme synthetic pathways originate from the precursor UPG III: the CPD pathway, the PPD pathway, and the siroheme-dependent pathway (21). In the CPD pathway, CPG III is converted by CgoX to CP III, while in the PPD pathway, CPG III is converted to PPG IX by CpdH/oxygen-dependent coprogen III oxidase (Fig. 4*A*). The bottleneck in the pull module was an extremely high accumulation of CP III in the UP-K1 strain (Fig. 3*F*), prompting

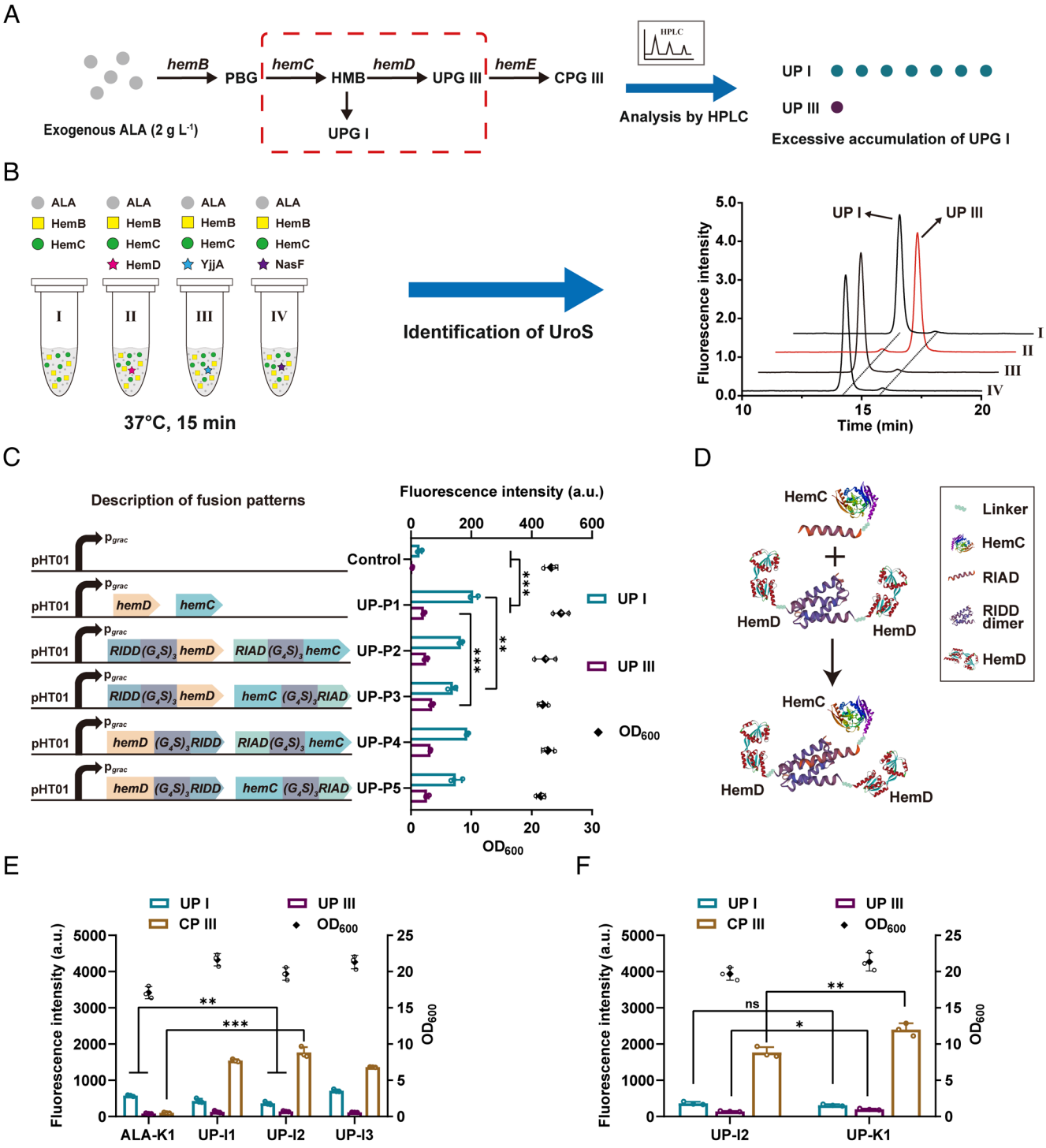

Fig. 3. Restraining competitive consumption of HMB to redirect metabolic flux toward heme synthesis. (*A*) Schematic illustration of MFA for the flow of ALA to CPG III, analyzed by HPLC. When the wild-type strain grew to 12 h, ALA (2 g L^{-1}) was supplemented, and the accumulations of UP I and UP III were monitored at 24 and 48 h by HPLC. The abbreviations are shown in Fig. 1. (*B*) Identification of UroS enzymes by constructing trienzymatic reaction system in vitro. Each of the different UroS (0.1 μmol of HemD, YjjA, or NasF) was incubated separately in 1 mL of 0.1 M Tris/HCl buffer at pH 8.0, containing 0.5 μmol of HemB, 0.5 μmol of HemC and 0.1 mmol of DTT. Then, 50 μmol ALA was added into the above system for 15 min at 37 °C. (*C*) Screening of fusion modes between short peptide tags and target proteins by exogenous addition of 2 g L^{-1} ALA. (*D*) The assembly of trienzyme units. The RIDD and RIAD were fused to the N terminus of HemD and C-terminus of HemC, respectively, spaced by a flexible linker. (*E*) Optimal promoter screening of the *RIDD-hemD-hemC-RIAD* cassette. Strains UP-I1 to I3 (constructed on the basis of the ALA-K1 strain): *amyE*::P_{sdhB}-*RIDD-hemD-hemC-RIAD*, *amyE*::P_{yvyD}-*RIDD-hemD-hemC-RIAD*, *amyE*::P_{556}-*RIDD-hemD-hemC-RIAD*, respectively. (*F*) Effect of knocking out the endogenous *hemC* gene without short peptide label on porphyrin accumulation. UP-K1 strain: knocking out the endogenous *hemC* gene from the UP-I2 strain. The bars and solid symbols present as mean values ± SD from three independent biological replicates (n = 3). Hollow circles represent individual data points. **P* < 0.05, ***P* < 0.01, ****P* < 0.001; ns, no significance.

an investigation into the capacity of the CPD and PPD pathways to synthesize heme. Genes in the CPD (endogenous *hemY*, *hemH*, and *hemQ*) and PPD (*hemF*, *hemG*, and *hemH'* from *E. coli* BL21) pathways were overexpressed using the high-copy number plasmid pMINI-gntR in the UP-I2 strain. Notably, the heme titer in the Heme-P2 strain at 72 h (UP-I2 strain harboring pMINI-gntR-hemYHQ) was higher than in the Heme-P1 strain (UP-I2 strain harboring pMINI-gntR-hemFGH') (Fig. 4*B*), suggesting

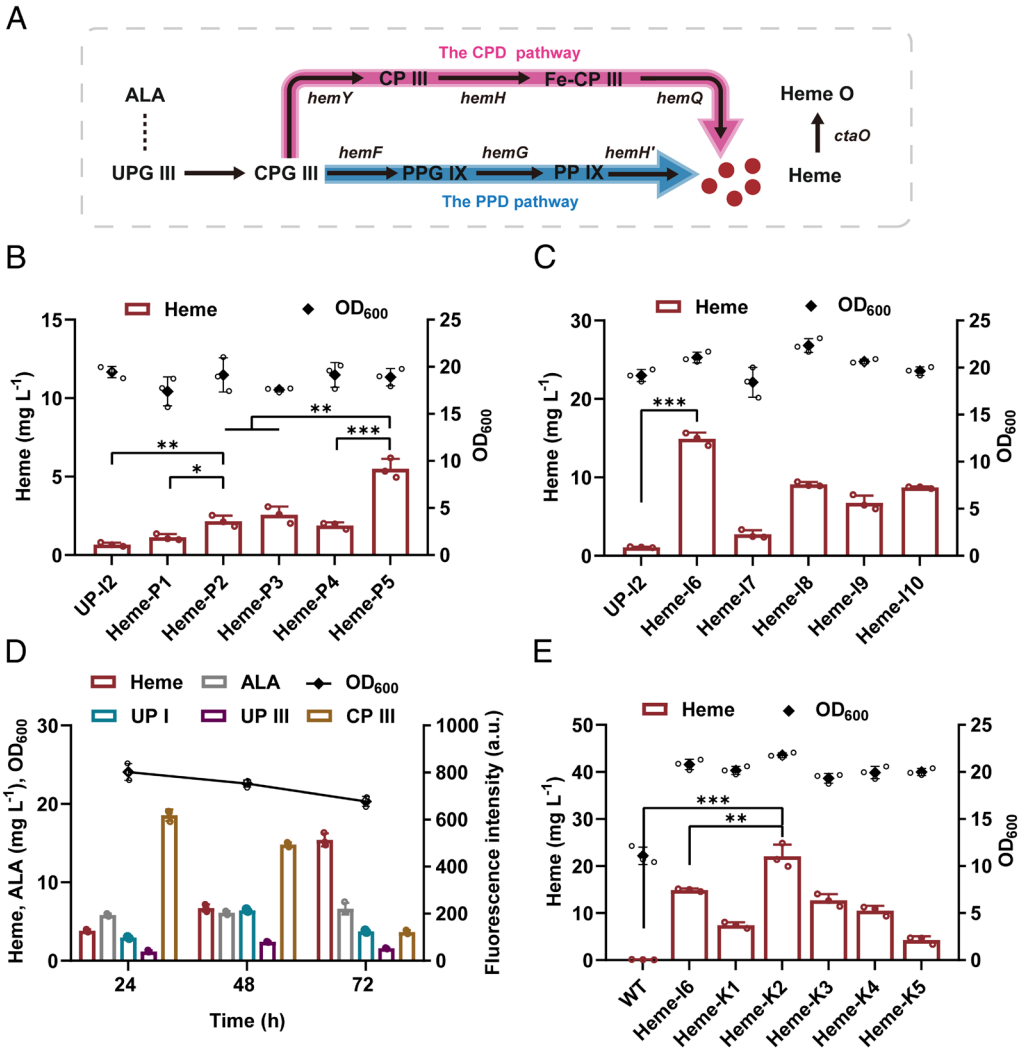

Fig. 4. Enhancing the rate-limiting steps in the CPD pathway to pull CPG III conversion to heme and eliminating heme utilization gene to block heme consumption. (*A*) Schematic illustration of the CPD pathway and the PPD pathway. Abbreviations: *hemF* encodes oxygen-independent CPG III oxidase; *hemG* encodes protoporphyrinogen oxidase; *hemH'* encodes protoporphyrin ferrochelatase. As shown in Fig. 1 for other abbreviations. (*B*) Comparison of the CPD and PPD pathways and identification of key rate-limiting enzymes in the CPD pathway. Strains Heme-P1 to P5 represent the UP-I2 strain harboring the plasmids pMINI-gntR-hemFGH', pMINI-gntR-hemYHQ, pMINI-gntR-hemH, pMINI-gntR-hemQH, and pMINI-gntR-hemQ, respectively. (*C*) Integrated expression of the *hemH-hemQ* cassette under the control of different promoters. Strains Heme-I6 to I10 (constructed on the basis of the UP-K1 strain): *amyE*::P_{333}-*hemH-hemQ*, *amyE*::P_{43}-*hemH-hemQ*, *amyE*::P_{556}-*hemH-hemQ*, *amyE*::P_{TP2}-*hemH-hemQ*, and *amyE*::P_{TP4}-*hemH-hemQ*, respectively. (*D*) Accumulations of key intermediates and cell growth (OD_{600}) of the Heme-I6 strain at 24, 48, and 72 h in shake-flask cultivation. (*E*) Effect of knocking out the genes catalyzing heme utilization on heme titer and OD_{600}. WT: wild-type *B. subtilis*; strains Heme-K1 to K5: knocking out the *ctaB*, *ctaO*, *hmoA*, *hmoB*, and *hmoA-hmoB* genes from the Heme-I6 strain, respectively. The bars and solid symbols present as mean values ± SD from three independent biological replicates (n = 3). Hollow circles represent individual data points. *$P < 0.05$, **$P < 0.01$, ***$P < 0.001$; ns, no significance.

that the endogenous CPD pathway was more suitable for heme biosynthesis in *B. subtilis*.

To identify the rate-limiting steps in the CPD pathway, the *hemH* and *hemQ* genes were separately or combinatorially overexpressed using the pMINI-gntR plasmid. Among the Heme-P3, Heme-P4, and Heme-P5 strains, which were the UP-I2 strain harboring pMINI-gntR-hemH, pMINI-gntR-hemHQ, and pMINI-gntR-hemQ, respectively, the Heme-P5 strain exhibited the highest heme titer (Fig. 4*B*). This result demonstrated that HemQ was a key rate-limiting enzyme in the CPD pathway. Subsequently, the *hemQ* gene was inserted into the *amyE* locus of the UP-K1 strain under the control of different promoters (P_{333}, P_{43}, P_{TP2}, P_{TP4}, and P_{556}). Among these five knock-in strains, the Heme-I1 strain exhibited the highest heme titer (2.60 ± 0.31 mg L^{-1}) (*SI Appendix*, Fig. S5*A*). However, there was still extensive CP III accumulation in the Heme-I1 strain (*SI Appendix*, Fig. S5*B*). Consequently, the endogenous *hemH* gene was inserted into the genome of strains Heme-I1 to Heme-I5, generating strains Heme-I6 to Heme-I10. The results showed that the heme titer in the Heme-I6 strain (the integrated *hemH* and *hemQ* genes under the control of P_{333}) reached 14.91 ± 0.80 mg L^{-1} at 72 h, representing a 13.55-fold increase compared with the titer in the UP-K1 strain (Fig. 4*C*). Meanwhile, the accumulation of CP III was reduced to a lower level in the Heme-I6 strain, decreasing by 94.81% compared with the level in the UP-K1 strain (*SI Appendix*, Fig. S6*A*). Significant differences in heme titers observed between chromosome integration and plasmid-based overexpression of the *hemH* and *hemQ* genes (Fig. 4 *B* and *C*) may result from excessive overexpression of the *hemH* gene, which disrupts cellular energy metabolism by interfering with iron metabolism, ultimately impairing heme synthesis (29, 44, 45). Due to the lower accumulation of CP III in the Heme-I6 strain (*SI Appendix*, Fig. S6*A*) and the adverse impacts of overexpressing the *hemY* gene (29), the conversion step of CPG III to CP III was not further engineered.

To determine whether excessive Fe-CP III accumulated in the Heme-I6 strain, the *hemQ* gene was overexpressed using a plasmid. The results showed a slight increase in heme titer (*SI Appendix*, Fig. S6*B*). As the growth of the Heme-I6-hemQ strain was inhibited (*SI Appendix*, Fig. S6*B*) and overexpression of the *hemQ* gene would impose additional metabolic burden, other engineering strategies were not pursued for the CPD pathway.

To confirm the effects of metabolic engineering in heme biosynthetic pathway, various intermediates in the Heme-I6 strain were monitored at 24, 48, and 72 h. There was no accumulation of porphobilinogen (PBG), and the accumulations of ALA, UP III, and CP III were at lower levels at 72 h (Fig. 4*D*), suggesting that the key bottlenecks in the heme synthetic pathway have been overcome. Additionally, compared with the ALA titer in the ALA-K1 strain, the ALA accumulation in the Heme-I6 strain decreased by 78.24% at 24 h (Figs. 2*C* and 4*D*). The UP III accumulation in the Heme-I6 strain decreased by 65.62% at 48 h compared with the UP III titer in the UP-K1 strain (Figs. 3*F* and 4*D*). These results support that even if the *hemB* and *hemE* genes were not overexpressed, the elimination of downstream bottlenecks would effectively alleviate the accumulations of ALA and UP III. In contrast, the expression of the *hemB* and *hemE* genes underwent extra enhancement in other reports (13, 14, 25), which may impose an additional metabolic burden on the host.

The inhibition of heme consumption was a useful strategy for improving heme supply (14, 25, 46). In *B. subtilis*, protoheme IX farnesyltransferase (encoded by the *ctaB* and *ctaO* genes) and heme monooxygenase (encoded by the *yetG* and *yhgC* genes) catalyze the downstream conversion of heme (47–49). A crucial point in the block module is reducing heme utilization by these enzymes. Consequently, the *ctaB*, *ctaO*, *yetG*, and *yhgC* genes were knocked out in the Heme-I6 strain, generating strains Heme-K1 to Heme-K4, respectively. The knockout of the *ctaO* gene (Heme-K2 strain) resulted in a 1.48-fold increase in heme titer compared to the titer in the Heme-I6 strain, reaching 22.06 ± 2.52 mg L^{-1} of total heme (including extracellular heme of 0.38 ± 0.13 mg L^{-1}) at 72 h (Fig. 4*E* and *SI Appendix*, Fig. S7*A*). This result indicates protoheme IX farnesyltransferase (encoded by the *ctaO* gene) plays a critical role in the consumption of heme in *B. subtilis*. However, the elimination of heme monooxygenase did not have a positive effect on the intracellular heme supply. It suggests that although the function of HmoA and HmoB to degrade heme has been verified in vitro, this may not be related to their in vivo function (48, 49). Finally, we successfully constructed an antibiotic marker-free chassis strain with limited intermediate accumulation and efficient heme supply, which outperformed the previous neomycin-resistant *B. subtilis* strain with higher intermediate accumulation and lower heme production (46). Notably, the heme titer (22.06 mg L^{-1}) in the Heme-K2 strain was significantly increased by 221-fold compared to that of the wild-type strain (WT). To evaluate the heme production capability of the Heme-K2 strain at scale, we conducted a 5-L fed-batch fermentation. The fermentation yielded a heme titer of 282.17 mg L^{-1} on day 6, the highest value reported to date in *B. subtilis* (*SI Appendix*, Fig. S8). Therefore, based on the better performance of heme supply in the Heme-K2 strain (*SI Appendix*, Fig. S7*B*), this engineered strain was used as the chassis cell to synthesize active Hb and Mb.

The Properties and Applications of Hb and Mb Synthesized in Engineered *B. subtilis*. Having developed a suitable expression system for Hb and Mb (*SI Appendix*, Text S1), the Heme-K2 strain was applied to efficiently synthesize active Hb and Mb. In shake-flask cultivation, the titers of S-Hb, C-Hb, B-Mb, and P-Mb reached 212.93 ± 9.92 mg L^{-1}, 218.34 ± 2.39 mg L^{-1}, 315.44 ± 2.50 mg L^{-1}, and 335.72 ± 7.73 mg L^{-1} at 24 h, which were 1.14-fold, 1.09-fold, 1.39-fold, and 1.21-fold higher than the corresponding titers in the wild-type strain, respectively (Fig. 5 *A* and *B*). The increased titers of Hb and Mb may be attributed to improved heme supply, which enhances their stability (50, 51).

Due to the wide applications of Hb and Mb in iron supplements, biocatalysis, and food-grade colorants and flavoring agents, it is essential to examine their spectral and enzymatic properties (1, 3, 7, 8). Commercial B-Hb and horse myoglobin (H-Mb) were used as reference standards to validate the properties of Hb and Mb synthesized in the engineered strain. First, the spectral properties of Hb and Mb at 280 to 700 nm were detected. The purified Hb and Mb exhibited Soret bands at 410 nm, consistent with the reference standards (Fig. 5*C*) and previously reported biosynthesized Hb and Mb (12–14). Furthermore, the Soret bands of Hb and Mb synthesized in the engineered strain were more prominent than those in the wild-type strain (*SI Appendix*, Fig. S9), suggesting that the Heme-K2 strain provided a more efficient heme supply for Hb and Mb. To confirm the improved heme supply, the heme-binding rates of Hb and Mb were measured by a pyridine hemochromagen assay (52). Compared with the wild-type strain, the heme-binding ratios of S-Hb, C-Hb, B-Mb, and P-Mb synthesized in the Heme-K2 strain increased by 3.66-fold, 5.40-fold, 1.81-fold, and 2.81-fold, reaching 54.58 ± 2.41%, 74.03 ± 4.13%, 40.51 ± 4.17%, and 43.04 ± 4.59%, respectively (Fig. 5*D*).

The excellent peroxidase activity (POD) is a crucial reason that Hb and Mb can be used in biocatalysis (53, 54). Here, the POD activities of these synthesized Hb and Mb were evaluated by using 3,3′,5,5′-tetramethylbenzidine (TMB), 2,2′-azino-di-(3-ethylbenzothiazoline-6-sulfonic acid) (ABTS), guaiacol, and *o*-phenylenediamine as substrates (55). The results showed that the peroxidase activities of Hb and Mb synthesized in the engineered strain were significantly improved compared with those obtained in the wild-type strain. Moreover, the S-Hb, C-Hb, B-Mb, and P-Mb synthesized in the engineered strain showed peroxidase activities similar to those of the native standard H-Mb and B-Hb (Fig. 5 *E* and *F* and *SI Appendix*, Fig. S 10 *A* and *B*). Therefore, the Hb and Mb biosynthesized in this study are suitable for commercial applications.

The color and flavor of meat are crucial indicator for assessing meat quality (8, 56). Both Hb and Mb play pivotal roles in the color and flavor of meat and can be applied to produce commercial plant-based meat analogs (5, 8, 9). Soy proteins are widely used as primary materials for artificial meat due to their cost-effectiveness and ready availability (57). To evaluate the impact of Hb and Mb synthesized in the Heme-K2 strain on the color and flavor of plant-based meat analogs, recombinant C-Hb and B-Mb were added to the soy protein isolate (SPI) at a ratio of 1 wt%. The antibacterial, antiviral, and potential anticancer properties of food-grade *B. subtilis* has been demonstrated (58), and it can serve as a host for vaccine production and delivery (59). Due to its safety and versatile characteristics, the cell lysates of *B. subtilis* containing equivalent concentrations of C-Hb and B-Mb were also directly added to SPI. Meanwhile, SPI samples containing 1% of commercial B-Hb and H-Mb were prepared as the positive controls. The color parameters (L*, a*, b*) of SPI samples were assessed after the addition of Hb and Mb. The results showed that the addition of purified proteins (pC-Hb and pB-Mb), cell lysates (lC-Hb and lB-Mb), and native standard proteins (sB-Hb and sH-Mb) exhibited similar tendency toward darkening and reddening (Table 1 and *SI Appendix*, Fig. S11*A*). Among them, the red intensity of pC-Hb was higher than that of sB-Hb, while the red intensity of pB-Mb was similar to that of sH-Mb. Additionally,

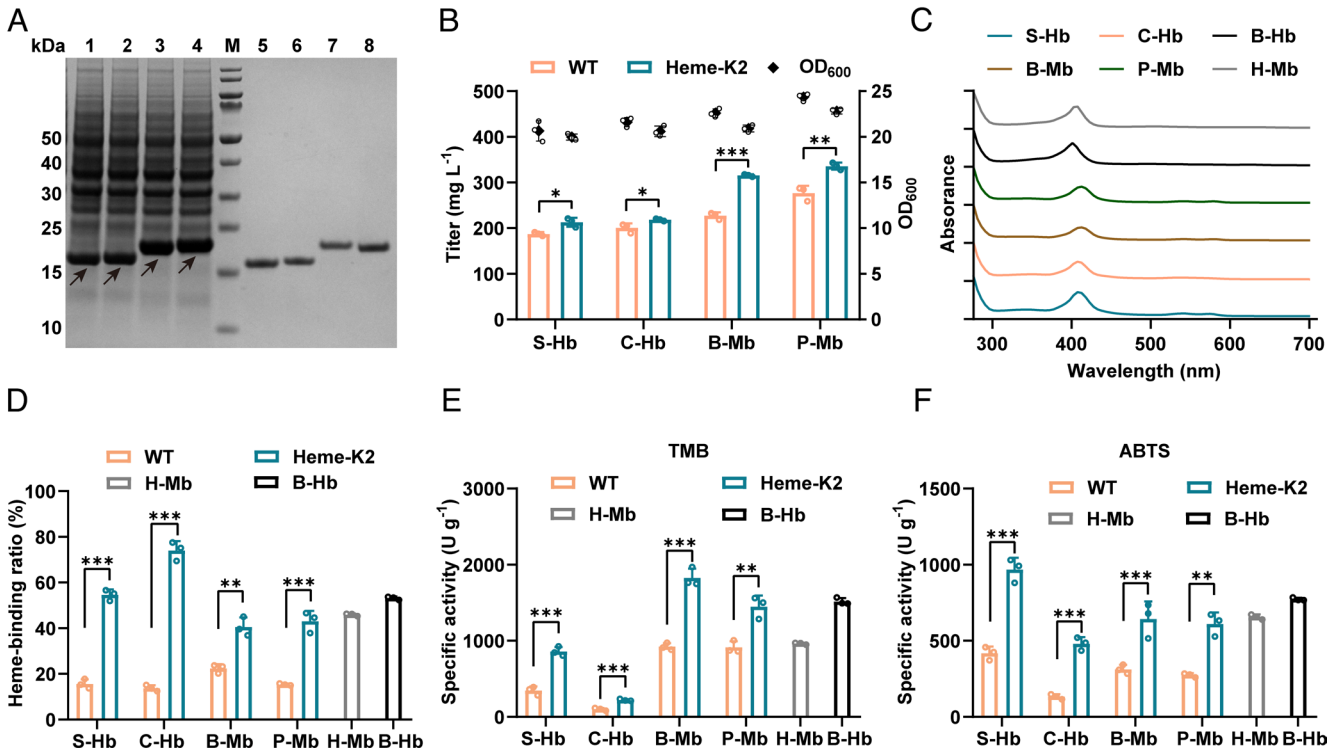

Fig. 5. The biochemical properties of Hb and Mb synthesized in the Heme-K2 strain in shake-flask cultivation. (*A*) SDS-PAGE analysis of Hb and Mb expressed in the Heme-K2 strain at 24 h. Lanes 1 to 4: intracellular synthesis of S-Hb, C-Hb, B-Mb, and P-Mb, respectively. Lanes 5 to 8: purified S-Hb, C-Hb, B-Mb, and P-Mb, respectively. Lane M: protein standard marker. The arrows indicate the Hb and Mb bands. The molecular weight of S-Hb, C-Hb, B-Mb, and P-Mb containing 6× His tags were 16.35, 16.52, 17.90, and 17.91 kDa, respectively. (*B*) Titer of Hb and Mb expressed in the WT (wild-type) and Heme-K2 strains at 24 h. (*C*) Spectral characteristics of purified Hb and Mb. (*D*) Heme-binding ratios of purified Hb and Mb. (*E* and *F*) Specific POD activities of purified Hb and Mb for TMB (*E*), ABTS (*F*). H-Mb and B-Hb: the reference standards horse myoglobin (H-Mb) and bovine hemoglobin (B-Hb). These purified Hb and Mb were synthesized in the WT (wild-type) and Heme-K2 strains, respectively, in shake-flask cultivation. The bars and solid symbols present as mean values ± SD from three independent biological replicates (n = 3). Hollow circles represent individual data points. **P* < 0.05, ***P* < 0.01, ****P* < 0.001; ns, no significance.

the red intensities of lC-Hb and lB-Mb were lower than those of sB-Hb and sH-Mb, but they still significantly outperformed the control without the addition of Hb or Mb. Besides, the SPI samples with the addition of Mb and Hb demonstrated favorable flavor characteristics (*SI Appendix*, Fig. S11 *B* and *C* and Text S2), presenting great potential for producing meat products such as sausage.

Production of Hb and Mb by Fed-Batch Fermentation. To further evaluate the applications of the Heme-K2 strain for producing Hb and Mb on a large-scale, fed-batch fermentation was performed in a 5 L bioreactor. However, this strain continuously consumed the gluconate inducer during the expression of Hb or Mb, which posed a hindrance to large-scale fermentation. Therefore, to reduce inducer consumption, the *gntK* gene (associated with gluconate utilization) was knocked out in the Heme-K2 strain to generate the Heme-K2-ΔgntK strain (60). The results demonstrated that the consumption rate of gluconate in the Heme-K2-ΔgntK strain significantly decreased, while the cell growth and the expression of S-Hb were not influenced (Fig. 6*A* and *SI Appendix*, Fig. S12). After optimizing the fermentation conditions, the Heme-K2-ΔgntK strain was used for the production of Hb and Mb (*SI Appendix*, Text S3). Fed-batch fermentations were conducted in the BSM medium and the expression of Hb or Mb was induced by sodium gluconate (40 g L^{-1}) at 4.5 h. Additionally, ammonium sulfate (24 g L^{-1}) and yeast extract (48 g L^{-1}) were supplemented at a constant rate from 6 h. The highest titers of Hb and Mb were obtained at 15 h of fed-batch fermentation. The titers of S-Hb, C-Hb, B-Mb, and P-Mb reached 0.81, 0.82, 1.11, and 1.01 g L^{-1} (Fig. 6 *B–E* and *SI Appendix*, Fig. S14), equivalent to the productivities of 54.00, 54.67, 73.33, and 67.33 mg L^{-1} h^{-1}, respectively. Compared with the WT-ΔgntK strain (wild-type strain with the *gntK* knockout), engineered strains harboring the plasmid to express hemoproteins exhibited 1.84-fold, 2.93-fold, 2.85-fold, and 1.84-fold increases in the titers of S-Hb, C-Hb, B-Mb, and P-Mb, respectively (Fig. 6 *B–E* and *SI Appendix*, Figs. S15 and S16 *A–D*). These results demonstrate the importance of increasing heme supply in the large-scale hemoprotein production. Even after scaling up the fermentation process, significant increases in heme-binding ratios and peroxidase activities were observed in the hemoproteins synthesized in the engineered strain (Fig. 6*F* and *SI Appendix*, Figs. S16 *E* and *F* and S17). Notably, these

Table 1. The color evaluation of SPIs with the addition of Mb and Hb

Group	Attribute		
	L* (lightness)	a* (redness)	b*(yellowness)
Control	40.55 ± 0.54^{a}	0.99 ± 0.29^{d}	8.82 ± 0.32^{a}
pC-Hb	33.61 ± 0.84^{c}	4.69 ± 0.14^{a}	7.36 ± 0.41^{b}
lC-Hb	35.51 ± 0.56^{b}	2.30 ± 0.15^{bc}	9.01 ± 0.38^{a}
B-Hb	33.14 ± 0.79^{c}	4.08 ± 0.27^{ab}	7.43 ± 0.68^{b}
pB-Mb	36.37 ± 0.89^{b}	3.24 ± 0.19^{b}	7.66 ± 0.48^{b}
lB-Mb	35.41 ± 0.75^{b}	2.11 ± 0.32^{c}	9.28 ± 0.69^{a}
H-Mb	33.23 ± 0.84^{c}	3.15 ± 0.10^{bc}	7.35 ± 0.61^{b}

Data are expressed as mean SD (n = 5). Values with different letters (a–d) in the same column differ significantly (*P* < 0.05). Control, no addition; pC-Hb, purified clover hemoglobin; lC-Hb, clover hemoglobin contained in cell lysate; sB-Hb, standard bovine hemoglobin; pB-Mb, purified bovine myoglobin; lB-Mb, bovine myoglobin contained in cell lysate; sH-Mb, standard horse myoglobin.

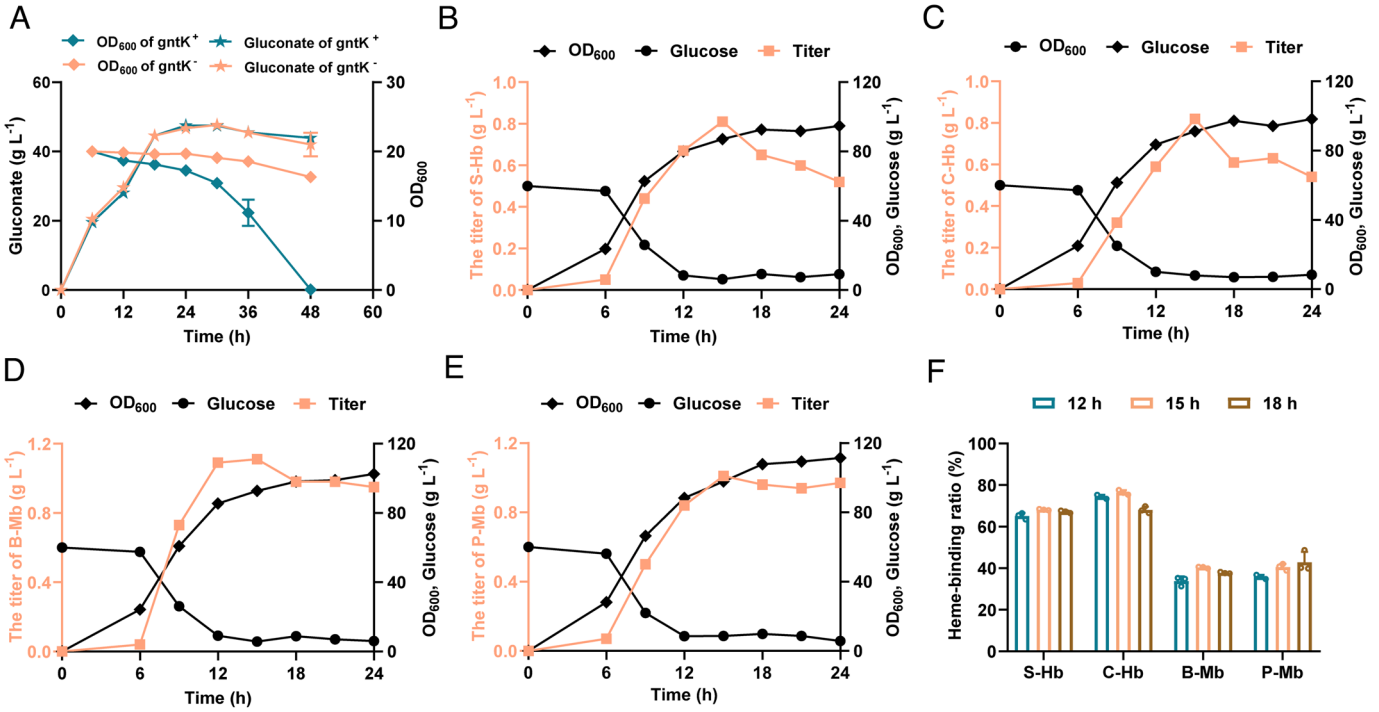

Fig. 6. Production of Hb and Mb in fed-batch fermentation. (*A*) Effect of the *gntK* gene knockout on gluconate consumption and OD_{600}. $gntK^+$ and $gntK^-$ represent the Heme-K2 and Heme-K2-ΔgntK strains, respectively. The bars and solid symbols present as mean values ± SD from three independent biological replicates (n = 3). (*B*–*E*) Titers of S-Hb (*B*), C-Hb (*C*), B-Mb (*D*), and P-Mb (*E*) in fed-batch fermentation of the Heme-K2-ΔgntK strain. (*F*) Heme-binding ratios of purified Hb and Mb. These purified Hb and Mb were synthesized in the Heme-K2-ΔgntK strain in fed-batch fermentation. The bars and solid symbols present as mean values ± SD from three independently detected values (n = 3). Hollow circles represent individual data points.

increases were comparable to those achieved in shake-flask cultivation. These excellent performances confirm the effectiveness and applicability of the Heme-K2-ΔgntK strain, highlighting its potential for industrial production of active hemoproteins.

Discussion

Hb and Mb are urgently demanded in the fields of food, medicine, and biocatalysts (1, 3, 5). With the rapid advances in metabolic engineering and synthetic biology, microbial synthesis of Hb and Mb has emerged as a promising strategy. However, the heme supply of wild-type strain has been insufficient to support the production of active Hb and Mb (13, 27). In this study, an engineered *B. subtilis* with efficient heme supply was constructed by increasing the supply of heme precursor ALA, minimizing the competitive consumption of HMB, selecting the CPD pathway as the superior downstream route for heme synthesis, enhancing the crucial rate-limiting steps, and blocking the utilization of heme. Subsequently, by adopting a suitable globin expression strategy, active S-Hb, C-Hb, B-Mb, and P-Mb could be synthesized in the engineered *B. subtilis* in shake-flask cultures and fed-batch fermentations. Importantly, these biosynthesized Hb and Mb demonstrated notable efficacy in improving the color and flavor of plant-based meat analogs.

The biosynthetic pathway of heme, along with its crucial rate-limiting steps, varies depending on the species (21). Therefore, customized strategies for specific species are recommended to achieve an efficient supply of heme. In this study, metabolic flux analysis was employed as a pivotal tool throughout the metabolic engineering process to explore the bottleneck of heme synthetic pathway and provide insightful guidance for the formulation of engineering strategies. Four bottlenecks have been identified as follows: I) insufficient supply of ALA, II) excessive consumption of HMB caused by autocyclization, III) inefficient conversion of the CPD pathway, and IV) massive consumption of heme catalyzed by protoheme IX farnesyltransferase. These findings have specified the bottlenecks in the heme synthetic pathway in *B. subtilis*. In contrast, the only report on the engineered *B. subtilis* for heme synthesis did not identify the last three bottlenecks (46).

The push and pull forces are indispensable in the complex cellular metabolic network (61). In this study, a combined strategy of "push" and "pull," along with "restrain" and "block," was implemented to address the bottlenecks mentioned above. First, the optimal endogenous C5 pathway was enhanced to push carbon flux toward the synthesis of precursor ALA. During this process, the ALA titer in the $HemA_{anti\text{-}feedback}$ strain (ALA-P2 strain) increased from 0 to 26.63 mg L^{-1} (Fig. 2*B*). The result indicates that the proteolysis of HemA is not confined to *E. coli* and *Salmonella typhimurium*, but also occurs in *B. subtilis* (25, 31). Second, after identifying HemD as the authentic UroS, the assembly of HemC and HemD significantly restrained the free diffusion of unstable HMB intermediates. This modification resulted in a 36.88% decrease in the accumulation of UP I by-product, alongside a 1.71-fold and 17.37-fold increase in the accumulations of UP III and CP III, respectively (Fig. 3*E*). These improvements may result from their assembly channeling PBG toward UPG III synthesis and facilitating an efficient catalytic cascade reaction (62, 63). Third, the conversion efficiency of CPG III via the CPD or PPD pathways has never been investigated in microbial cells. In this study, the higher efficiency in the CPD pathway was confirmed in *B. subtilis* (Fig. 4*B*). This result is also supported by the fact that ΔG0' of the CPD pathway in *C. glutamicum* is lower than that of the PPD pathway in *E. coli* (29). Additionally, another reason was the lower transcription levels of enzymes, particularly for HemF, involved in the PPD pathway of *E. coli* when expressed in *B. subtilis* (*SI Appendix*, Fig. S18). Moreover, HemH and HemQ,

identified as key rate-limiting enzymes in the CPD pathway, were enhanced to pull the flux of CPG III toward the synthesis of heme, with a 13.55-fold increase in the titer of heme (Fig. 4 *B* and *C*). However, previous attempts to engineer the heme biosynthesis pathway in *B. subtilis* have ignored these critical metabolic bottlenecks (46). Finally, protoheme IX farnesyltransferase (encoded by the *ctaO* gene) was eliminated to block the consumption of heme, resulting in a 47.95% increase in the titer of heme (Fig. 4*E*). In contrast, the previous studies focused on increasing the heme titer by eliminating dye-decolorizing peroxidase and heme oxygenase (14, 25, 46).

The reprogramming of microbial metabolism to produce valuable compounds often results in metabolic burden, accompanied by adverse physiological effects (26, 27, 64). Efforts have been undertaken to balance the cellular resources allocated for synthesizing heme and hemoprotein by applying heme biosensors (13, 27). However, these biosensors only regulate the transcription of the *hemB* gene to trade off heme synthesis, without sufficiently considering the related metabolic burden. In our study, the optimization of promoter and chromosomal integration were employed in the metabolic engineering of the heme synthetic pathway to alleviate metabolic burden and enhance cellular resource allocation for synthesizing Hb and Mb. Based on the "push–pull" theory and the observed limited accumulation of the intermediates ALA, UP III, and CP III during the metabolic engineering, the *hemB*, *hemE*, and *hemY* genes were not overexpressed, in contrast to the previous strategies (13, 14, 25, 26, 29), thereby further reducing the cellular metabolic burden. Ultimately, the "push–restrain–pull–block" strategy drove 221-fold improvement of heme titer in shake-flask fermentation and achieved the highest reported titer (282.17 mg L^{-1} in 5-L fed-batch fermentation) to date in *B. subtilis* (*SI Appendix*, Fig. S8).

Using the stable and antibiotic marker-free Heme-K2-ΔgntK strain with efficient heme supply, the highest titers and productivities of S-Hb, C-Hb, B-Mb, and P-Mb during a 5 L fed-batch fermentation process were achieved (Fig. 6 *B*–*E*). Compared to the WT-ΔgntK strain used for hemoprotein production under fed-batch fermentation (*SI Appendix*, Fig. S16 *A*–*D*), the engineered strains exhibited 1.84-fold, 2.93-fold, 2.85-fold, and 1.84-fold higher titers of S-Hb, C-Hb, B-Mb, and P-Mb, respectively. These findings are consistent with previous studies and demonstrate that enhancing heme supply significantly improves the production of hemoproteins (15, 16, 27). This study represents a report of high-titer synthesis of these Hb and Mb in *B. subtilis*. Among them, the titers of C-Hb, B-Mb, and P-Mb reached 0.82 g L^{-1},1.11 g L^{-1}, and 1.01 g L^{-1}, respectively, marking a significant enhancement by 60.00-fold, 16.11-fold, and 3.37-fold compared to the previously reported highest titers achieved in yeasts (14, 16). Meanwhile, the fermentation period for Hb and Mb synthesis was significantly shortened from 72 to 96 h in yeast to only 15 h in *B. subtilis*, reducing the risks of fermentation contamination and production costs. Moreover, these hemoproteins demonstrated properties similar to those of native H-Mb and B-Hb. In the future, metabolic engineering strategies, such as identifying and knocking out genes encoding proteases which function to degrade hemoprotein, as well as overexpressing heme chaperones to improve the incorporation of heme into globin, could be adopted to further improve hemoglobin production.

With the efficient heme supply, the Heme-K2-ΔgntK strain can also be applied for synthesizing P450-BM3. This strain exhibited a 1.53-fold increase in P450-BM3 titer and a 3.64-fold increase in whole-cell catalytic activity for phenol compared to the wild-type strain (*SI Appendix*, Fig. S19), suggesting that the engineered *B. subtilis* chassis can serve as a universal platform for synthesizing other hemoproteins. Additionally, the SPI samples with the addition of C-Hb and B-Mb exhibited prominent darkening and reddening (Table 1 and *SI Appendix*, Fig. S11*A*), as well as rich meat flavor (*SI Appendix*, Fig. S11 *B* and *C*), indicating the notable efficacy of biosynthesized Hb and Mb as color and flavor additives. Among them, C-Hb exhibited the most significant effectiveness, attributed to its high heme-binding rate and retention of red color even under oxidized conditions (10). Due to the food safety of *B. subtilis* and the effectiveness of cell lysates as colorants, the direct use of cell lysates containing synthesized C-Hb and B-Mb will substantially reduce production costs. Overall, our strategy paves the way for the microbial synthesis and commercial application of heme and high value-added hemoproteins.

Materials and Methods

All of the materials and methods used in this study are detailed in *SI Appendix, Materials and Methods*. This includes chemical reagents, media and growth conditions, genetic manipulations, construction of plasmids, purification and quantification of proteins, detection of heme-binding ratios and enzymatic activities, construction of the trienzymatic reaction system, preparation of the SPI samples, analytical procedures, strains and plasmids, and sequences of primers and sgRNAs.

Data, Materials, and Software Availability. All study data are included in the article and/or *SI Appendix*.

ACKNOWLEDGMENTS. This work was supported by the National Key Research and Development Program of China (2021YFC2101400), the National Natural Science Foundation of China (31900067), and the National First-class Discipline Program of Light Industry Technology and Engineering (LITE2018-08). S.Y.L. was supported by the Development of platform technologies of microbial cell factories for the next-generation biorefineries project (2022M3J5A1056117) from National Research Foundation supported by the Korean Ministry of Science and Information and Communication Technology.

Author affiliations: [a]Science Center for Future Foods, Jiangnan University, Wuxi, Jiangsu 214122, China; [b]Key Laboratory of Industrial Biotechnology, Ministry of Education, School of Biotechnology, Jiangnan University, Wuxi, Jiangsu 214122, China; [c]Jiangsu Province Engineering Research Center of Food Synthetic Biotechnology, Jiangnan University, Wuxi, Jiangsu 214122, China; [d]Engineering Research Center of Ministry of Education on Food Synthetic Biotechnology, Jiangnan University, Wuxi, Jiangsu 214122, China; [e]Key Laboratory of Molecular Enzymology and Engineering of Ministry of Education, School of Life Sciences, Jilin University, Changchun, Jilin 130023, China; and [f]Department of Chemical and Biomolecular Engineering (Brain Korea 21 four), Metabolic and Biomolecular Engineering National Research Laboratory and Systems Metabolic Engineering and Systems Healthcare Cross- Generation Collaborative Laboratory, Korea Advanced Institute of Science and Technology, Daejeon 34141, Republic of Korea

Author contributions: S.W., J.Z., J.L., J.C., G.D., Z.L., S.Y.L., and X.Z. designed research; S.W. and X.Z. performed research; S.W. and X.Z. analyzed data; J.Z., J.L., J.C., G.D., Z.L., and S.Y.L. conceived and supervised; and S.W., S.Y.L., and X.Z. wrote the paper.

1. I. C. Anderson *et al.*, Catalyzing PET-RAFT polymerizations using inherently photoactive zinc myoglobin. *Angew. Chem. Int. Ed. Engl.* **64**, e202414431 (2025).
2. Y. Jia *et al.*, Hemoglobin-based nanoarchitectonic assemblies as oxygen carriers. *Adv. Mater.* **28**, 1312–1318 (2016).
3. R. Yang *et al.*, Structure, properties and multifaceted food applications of four typical iron-binding proteins. *Food Hydrocolloids* **163**, 111080 (2025).
4. S. P. Suman, P. Joseph, Myoglobin chemistry and meat color. *Annu. Rev. Food Sci. Technol.* **4**, 79–99 (2013).
5. R. Simsa *et al.*, Extracellular heme proteins influence bovine myosatellite cell proliferation and the color of cell-based meat. *Foods* **8**, 521 (2019).
6. R. Z. Fraser *et al.*, Safety evaluation of soy leghemoglobin protein preparation derived from *Pichia pastoris*, intended for use as a flavor catalyst in plant-based meat. *Int. J. Toxicol.* **37**, 241–262 (2018).

7. J. Devaere *et al.*, Improving the aromatic profile of plant-based meat alternatives: Effect of myoglobin addition on volatiles. *Foods* **11**, 1985 (2022).
8. R. Fraser, P. O'Reilly Brown, J. Karr, C. Holz-Schietiger, E. Cohn, "Methods and compositions for affecting the flavor and aroma profile of consumables." US Patent 9700067B2 (2017).
9. D. Uzunalioglu, A. Yee, "Meat alternative formulation." WO Patent 2022187736A1 (2021).
10. M. P. Richards, M. Hargrove, S. Erazo-Castrejón, J. Alagurajan, "Compositions and methods for stabilizing meat substitute products." US Patent 2019200650A1 (2017).
11. T. J. Wright, R. W. Davis, Myoglobin extraction from mammalian skeletal muscle and oxygen affinity determination under physiological conditions. *Protein Expr. Purif.* **107**, 50–55 (2015).
12. O. V. Kosmachevskaya *et al.*, Expressed soybean leghemoglobin: Effect on *Escherichia coli* at oxidative and nitrosative stress. *Molecules* **26**, 7207 (2021).
13. F. Yu *et al.*, Biosynthesis of high-active hemoproteins by the efficient heme-supply *Pichia pastoris* chassis. *Adv. Sci.* **10**, e2302826 (2023).
14. J. K. Xue *et al.*, Systematic engineering of *Saccharomyces cerevisiae* for efficient synthesis of hemoglobins and myoglobins. *Bioresour. Technol.* **370**, 128556 (2023).
15. T. Tian *et al.*, High-level expression of leghemoglobin in *Kluyveromyces marxianus* by remodeling the heme metabolism pathway. *Front. Bioeng. Biotechnol.* **11**, 1329016 (2024).
16. F. Yu *et al.*, Developing a novel heme biosensor to produce high-active hemoproteins in *Pichia pastoris* through comparative transcriptomics. *Metab. Eng.* **84**, 59–68 (2024).
17. B. J. Z. Smith *et al.*, Development of a method to produce hemoglobin in a bioreactor culture of *Escherichia coli* BL21(DE3) transformed with a plasmid containing *Plesiomonas shigelloides* heme transport genes and modified human hemoglobin genes. *Appl. Environ. Microbiol.* **77**, 6703–6705 (2011).
18. K. Zhang *et al.*, Recent advances in recombinant protein production by *Bacillus subtilis*. *Annu. Rev. Food Sci. Technol.* **11**, 295–318 (2020).
19. Y. Su *et al.*, *Bacillus subtilis*: A universal cell factory for industry, agriculture, biomaterials and medicine. *Microb. Cell Fact.* **19**, 173 (2020).
20. N. Grosjean *et al.*, A hemoprotein with a zinc-mirror heme site ties heme availability to carbon metabolism in cyanobacteria. *Nat. Commun.* **15**, 3167 (2024).
21. S. Yang *et al.*, Recent advances in microbial synthesis of free heme. *Appl. Microbiol. Biotechnol.* **108**, 68 (2024).
22. H. A. Dailey *et al.*, Noncanonical coproporphyrin-dependent bacterial heme biosynthesis pathway that does not use protoporphyrin. *Proc. Natl. Acad. Sci. U.S.A.* **112**, 2210–2215 (2015).
23. T. Mingers *et al.*, The alternative coproporphyrinogen III oxidase (CgoN) catalyzes the oxygen-independent conversion of coproporphyrinogen III into coproporphyrin III. *Front. Microbiol.* **15**, 1378989 (2024).
24. S. B. Cardillo *et al.*, Uga3 and Uga35/Dal81 transcription factors regulate transcription in response to γ-aminobutyric acid and leucine. *Eukaryotic Cell* **9**, 1262–1271 (2010).
25. X. R. Zhao *et al.*, Metabolic engineering of *Escherichia coli* for secretory production of free haem. *Nat. Catal.* **1**, 720–728 (2018).
26. O. P. Ishchuka, *et al.*, Genome-scale modeling drives 70-fold improvement of intracellular heme production in *Saccharomyces cerevisiae*. *Proc. Natl. Acad. Sci. U.S.A.* **119**, e2108245119 (2022).
27. B. Hu *et al.*, Whole-cell P450 biocatalysis using engineered *Escherichia coli* with fine-tuned heme biosynthesis. *Adv. Sci.* **10**, e2205580 (2022).
28. J. Z. Ge *et al.*, Engineering *Escherichia coli* for efficient assembly of heme proteins. *Microb. Cell Fact.* **22**, 59 (2023).
29. Y. J. Ko *et al.*, Animal-free heme production for artificial meat in *Corynebacterium glutamicum* via systems metabolic and membrane engineering. *Metab. Eng.* **66**, 217–228 (2021).
30. S. J. Kwon *et al.*, High-level production of porphyrins in metabolically engineered *Escherichia coli*: Systematic extension of a pathway assembled from overexpressed genes involved in heme biosynthesis. *Appl. Environ. Microbiol.* **69**, 4875–4883 (2003).
31. L. Y. Wang *et al.*, A mutant HemA protein with positive charge close to the N terminus is stabilized against heme-regulated proteolysis in *Salmonella typhimurium*. *J. Bacteriol.* **181**, 6033–6041 (1999).
32. S. Yilmaz *et al.*, Towards next-generation cell factories by rational genome-scale engineering. *Nat. Catal.* **5**, 751–765 (2022).
33. M. Wong *et al.*, Modular optimization in metabolic engineering. *Crit. Rev. Biochem. Mol. Biol.* **56**, 587–602 (2021).
34. I. Schröder *et al.*, The *hemX* gene of the *Bacillus subtilis hemAXCDBL* operon encodes a membrane protein, negatively affecting the steady-state cellular concentration of HemA (glutamyl-tRNA reductase). *Microbiology (Reading)* **140**, 731–740 (1994).
35. K. Wang *et al.*, Engineering the lipid and fatty acid metabolism in yarrowia lipolytica for sustainable production of high oleic oils. *ACS Synth. Biol.* **11**, 1542–1554 (2022).
36. H. L. Schubert *et al.*, Structure and mechanistic implications of a uroporphyrinogen III synthase-product complex. *Biochemistry* **47**, 8648–8655 (2008).
37. N. Li *et al.*, Active studies of rat hydroxymethylbilane synthase. *Bioorg. Chem.* **36**, 241–251 (2008).
38. R. M. Jones, P. M. Jordan, Purification and properties of porphobilinogen deaminase from *Arabidopsis thaliana*. *Biochem. J.* **299**, 895–902 (1994).
39. G. N. Sarma *et al.*, Structure of D-AKAP2:PKA RI complex: Insights into AKAP specificity and selectivity. *Structure* **18**, 155–166 (2010).
40. W. Kang *et al.*, Modular enzyme assembly for enhanced cascade biocatalysis and metabolic flux. *Nat. Commun.* **10**, 4248 (2019).
41. Y. Q. Wang *et al.*, Enhancement of phycocyanobilin biosynthesis in *Escherichia coli* by strengthening the supply of precursor and artificially self-assembly complex. *Synth. Syst. Biotechnol.* **8**, 227–234 (2023).
42. E. Raux *et al.*, Identification and active analysis of enzymes required for precorrin-2 dehydrogenation and metal ion insertion in the biosynthesis of sirohaem and cobalamin in *Bacillus megaterium*. *Biochem. J.* **370**, 505–516 (2003).
43. F. Blanche *et al.*, Purification and characterization of S-adenosyl-L-methionine: Uroporphyrinogen III methyltransferase from *Pseudomonas denitrificans*. *J. Bacteriol.* **171**, 4222–4231 (1989).
44. S. Adinolfi *et al.*, Molecular insights into frataxin-mediated iron supply for heme biosynthesis in *Bacillus subtilis*. *PLoS One* **10**, e0122538 (2015).
45. C. H. Steingard, J. D. Helmann, Meddling with metal sensors: Fur-family proteins as signaling hubs. *J. Bacteriol.* **205**, e0002223 (2023)
46. S. M. Yang *et al.*, Improved biosynthesis of heme in *Bacillus subtilis* through metabolic engineering assisted fed-batch fermentation. *Microb. Cell Fact.* **22**, 102 (2023).
47. M. Throne-Holst, L. Hederstedt, The *Bacillus subtilis ctaB* paralogue, *yjdK*, can complement the heme A synthesis deficiency of a CtaB-deficient mutant. *FEMS Microbiol. Lett.* **183**, 247–251 (2000).
48. A. Gaballa, J. D. Helmann, *Bacillus subtilis* Fur represses one of two paralogous haem-degrading monooxygenases. *Microbiology* **157**, 3221–3231 (2011).
49. S. Park *et al.*, Structural and biochemical study of *Bacillus subtilis* HmoB in complex with heme. *Biochem. Biophys. Res. Commun.* **446**, 286–291 (2014).
50. C. J. Reedy, B. R. Gibney, Heme protein assemblies. *Chem. Rev.* **104**, 617–649 (2004).
51. H. F. Ji *et al.*, The effect of heme on the conformational stability of micro-myoglobin. *FEBS J.* **275**, 89–96 (2008).
52. I. Barr, F. Guo, Pyridine hemochromagen assay for determining the concentration of heme in purified protein solutions. *Bio. Protoc.* **5**, e1594 (2015).
53. Y. Kagawa *et al.*, Redox engineering of myoglobin by cofactor substitution to enhance cyclopropanation reactivity. *Angew. Chem. Int. Ed. Engl.* **63**, e202403485 (2024).
54. H. Keum *et al.*, Hemoglobin peroxidase reaction of hemoglobin efficiently catalyzes oxidation of benzo[a]pyrene. *Chemosphere* **268**, 128795 (2021).
55. N. Ma *et al.*, Switching an artificial P450 peroxygenase into peroxidase via mechanism-guided protein engineering. *ACS Catal.* **11**, 8449–8455 (2021).
56. C. H. Trinderup, Y. H. B. Kim, Fresh meat color evaluation using a structured light imaging system. *Food Res. Int.* **71**, 100–107 (2015).
57. R. Chantanuson *et al.*, Preparation of soy protein-based food gels and control of fibrous structure and rheological property by freezing. *Food Struct.* **32**, 100258 (2022).
58. N. K. Lee *et al.*, *Bacillus* strains as human probiotics: Characterization, safety, microbiome, and probiotic carrier. *Food Sci. Biotechnol.* **28**, 1297–1305 (2019).
59. S. Rosales-Mendoza, C. Angulo, *Bacillus subtilis* comes of age as a vaccine production host and delivery vehicle. *Expert Rev. Vaccines* **14**, 1135–1148 (2015).
60. Y. Fujita, T. Fujita, The gluconate operon gnt of *Bacillus subtilis* encodes its own transcriptional negative regulator. *Proc. Natl. Acad. Sci. U.S.A.* **84**, 4524–4528 (1987).
61. G. Jiang *et al.*, A "push-pull-restrain" strategy to improve citronellol production in *Saccharomyces cerevisiae*. *Metab. Eng.* **66**, 51–59 (2021).
62. F. Zhu *et al.*, Metabolic engineering of *Escherichia coli* for quinolinic acid production by assembling l-aspartate oxidase and quinolinate synthase as an enzyme complex. *Metab. Eng.* **67**, 164–172 (2021).
63. W. Xu *et al.*, Emerging molecular biology tools and strategies for engineering natural product biosynthesis. *Metab. Eng. Commun.* **10**, e00108 (2020).
64. J. Mao *et al.*, Relieving metabolic burden to improve robustness and bioproduction by industrial microorganisms. *Biotechnol. Adv.* **74**, 108401 (2024).